

Silicon Polarization Splitter and Rotator with Tolerance to Width Variations Using a Nonlinearly- Tapered and Partially-Etched Directional Coupler

Yong Zhang, Qingming Zhu, Yu He, and Yikai Su

State Key Lab of Advanced Optical Communication Systems and Networks, Department of Electronic Engineering,
Shanghai Jiao Tong University, Shanghai 200240, China
Author e-mail address: yikaisu@sjtu.edu.cn

Abstract: A silicon polarization splitter and rotator is experimentally demonstrated using a nonlinearly-tapered directional coupler. Adiabatic polarization splitting and rotating are achieved over a length of 129 μm . Fabrication tolerance to waveguide widths is also verified.

OCIS codes: (230.3120) Integrated Optics; (230.5440) Polarization-selective devices.

1. Introduction

The high index contrast of silicon nano-waveguides leads to high polarization dependence of silicon photonic devices. A polarization-diversity scheme was proposed to solve this problem [1]. As an essential building block, the polarization beam splitter and rotator (PSR) plays an important role in this scheme. Many types of silicon PSRs have been investigated and demonstrated in recent years, including those based on asymmetrical directional coupler [2], multimode interference [3], mode order conversion [4], and so on. Cross-polarization coupling can occur if the vertical and horizontal symmetries of the device structure are broken, then one polarization can be effectively rotated to the other. Directional-coupler-based PSRs were successfully demonstrated [5-7]. However, these PSRs required air as the upper-cladding to break the vertical symmetry. A PSR based on a double-etched directional coupler with a 130-nm shallow etching was successfully demonstrated with SiO_2 upper-cladding [8]. However, the PSR was sensitive to fabrication variation, and the bandwidth is limited. Recently, a PSR based on a linearly-tapered directional coupler was demonstrated with high fabrication tolerance and large bandwidth [9]. The coupling length was $\sim 700 \mu\text{m}$ to achieve adiabatic coupling.

In this paper, we experimentally demonstrate a silicon polarization splitter and rotator with a short coupling length and high fabrication tolerance using a nonlinearly-tapered partially-etched directional coupler. Attributed to the shortcuts-to-adiabaticity technique [10], the mode evolution is close to the adiabatic state in the nonlinearly-tapered directional coupler, leading to high-efficiency polarization splitting and rotating over a relatively short length of 129 μm . The vertical symmetry is broken by the partially-etched waveguide with the upper-cladding of SiO_2 . Such a PSR can be integrated with active silicon devices. The measured TM-to-TE conversion loss of the fabricated PSR is lower than 1.4 dB, and the insertion loss for the TE polarization is less than 0.5 dB in a wavelength range of 1508 nm \sim 1588 nm. The crosstalk values are below -24 dB and -18 dB for the TE and TM polarizations over the wavelength range of 80 nm, respectively. The demonstrated PSR exhibits tolerance to waveguide width variations. The TM-to-TE conversion losses are less than 0.3 dB at 1550nm for the slab width variations of ± 10 nm. As the width of the nonlinear-tapered waveguide is changed by +10 nm and -10 nm, the TM-to-TE conversion losses can be kept lower than 0.7 dB.

2. Device design and fabrication

The schematic structure of the proposed PSR is plotted in Fig. 1(a). The PSR device is designed on a silicon-on-insulator (SOI) wafer with a top silicon layer of 220 nm and upper/bottom SiO_2 cladding. The operation principle is based on the mode evolution between a nonlinearly-tapered waveguide and a partially-etched waveguide. To achieve an efficient TM-TE cross-polarization conversion, both horizontal and vertical symmetries need to be broken. A partially-etched waveguide is used in our work to break the vertical symmetry. The width of the partially-etched waveguide (w_2) is 390 nm, the partially-etched slab width (w_3) is 200 nm, and the partially-etched slab thickness (H) is 90 nm. The nonlinearly-tapered waveguide width $w_1(x)$ and the center-to-center waveguide spacing $D(x)$ change along the propagation direction. Under the scalar and paraxial approximations and weak coupling, the coupled mode equation can describe the mode amplitudes in the waveguides [10]:

$$\frac{d}{dx} \begin{bmatrix} A_0 \\ A_m \end{bmatrix} = -i \begin{bmatrix} -\Delta(x) & \kappa(x) \\ \kappa(x) & \Delta(x) \end{bmatrix} \begin{bmatrix} A_0 \\ A_m \end{bmatrix} \quad (1)$$

where A_0 and A_m are the amplitudes of the modes in the nonlinearly-tapered waveguide and the partially-etched waveguide, respectively, $\kappa(x)$ is the coupling coefficient, $\Delta(x) = [\beta_1(x) - \beta_2(x)] / 2$ denotes the propagation-constant mismatch between the waveguides. Following the invariant-based shortcuts-to-adiabaticity scheme and considering 100% adiabatic coupling, mathematical functions satisfying the desired initial and final states [10] can be chosen to derive the coupling coefficient $\kappa(x)$ and the mismatch $\Delta(x)$. The relation between the coupling coefficient κ and the spacing D , and the mismatch Δ versus the waveguide width w are simulated by the three-dimensional finite-difference time-domain (3D FDTD) method with fitting curves, as shown in Fig. 1(b) and 1(c). Using these relations and Eq. (1), we can calculate the spacing $D(x)$ and the waveguide width $w_1(x)$ along the propagation direction for the PSR, as shown in Fig. 1(d). The rapidly changes of $D(x)$ at the beginning and the end of the coupler lead to small waveguide bends and large propagation loss. If we do not consider the rapidly changing parts of $D > 1.287 \mu\text{m}$, the coupling length (L) is about $129 \mu\text{m}$. The length (L_c) of a taper after the partially-etched waveguide is $5 \mu\text{m}$, which is used to transform the partially-etched waveguide into a strip waveguide.

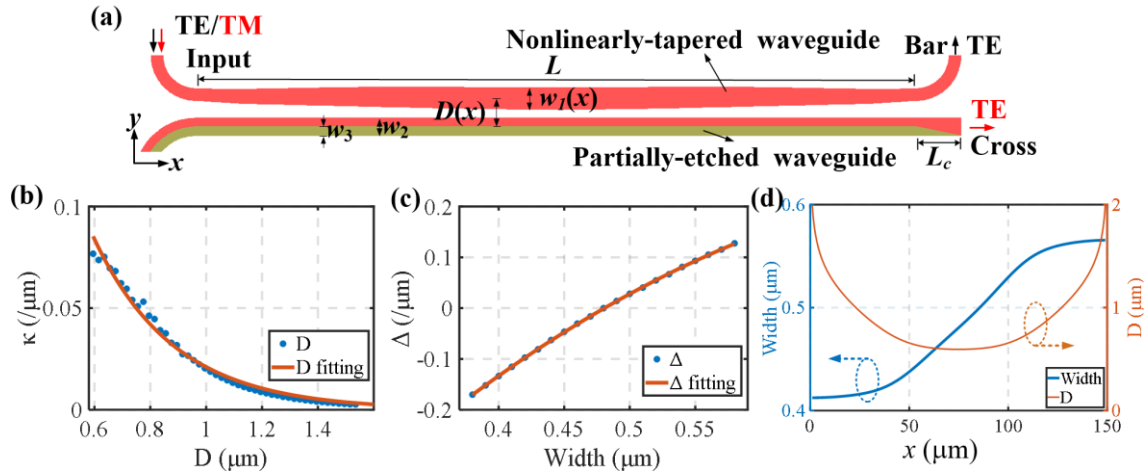


Fig. 1 (a) Schematic structure of the nonlinearly-tapered PSR. (b) Relation between κ and D ; (c) Relation between mismatch Δ and width w_1 . (d) Calculated $D(x)$ and $w_1(x)$ along the propagation direction for the PSR.

Figure 2 shows the simulated power distributions for the TE- and TM- polarized light inputs, respectively. When the TM-polarized light is injected, it is coupled to the partially-etched waveguide and simultaneously converted to the TE-polarized light, which then exists at the cross port. While for the case of TE-polarized light input, the light passes through the nonlinearly-tapered waveguide and outputs at the bar port. In the experiment, E-beam lithography (Vistec EBPG 5200⁺), inductively coupled plasma dry etching and plasma enhanced chemical vapor deposition were used to define the PSR structures on a SOI wafer. Magnified optical micrograph and scanning electron microscope (SEM) images of the fabricated PSR are shown in Fig. 3. In the measurements, TE- and TM- polarized lights from a tunable laser are coupled into/out of the chip by grating couplers, respectively. Two identical PSRs were fabricated to measure the responses for the TE- and TM- polarized light inputs, respectively.

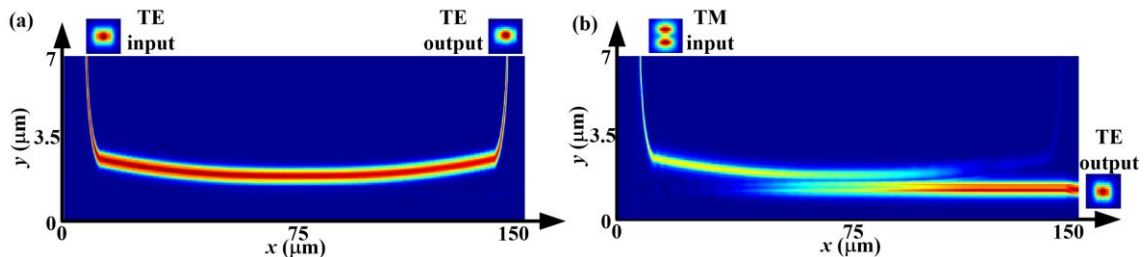


Fig. 2 Simulated power distributions for the (a) TE- polarized; and (b) TM-polarized light inputs, respectively.

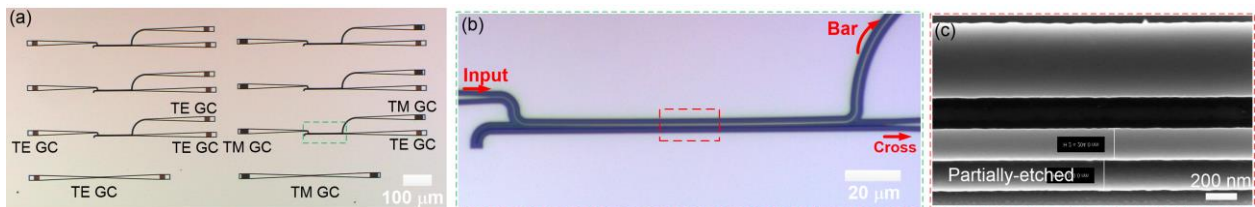


Fig. 3 (a) Optical micrograph of the fabricated devices. (b) Magnified optical micrograph of a PSR. (c) SEM photo of a fabricated PSR.

3. Measurement results

Figures 4(a) and 4(b) show the measured responses of the fabricated PSRs for the TE- and TM- polarized light inputs, respectively. For the TE input, the insertion loss is < 0.5 dB, and the crosstalk value is below -24 dB in a wavelength range of 1508 nm \sim 1588 nm. For the TM-polarized light, the TM-to-TE conversion loss is lower than 1.4 dB, and the crosstalk value is below -18 dB in the wavelength range of 80 nm. We also experimentally verified the fabrication tolerance by varying the nonlinearly-tapered waveguide width $w_1(x)$ and the slab width w_3 . As shown in Fig. 5(a), the TM-to-TE conversion losses are less than 0.3 dB and the crosstalk values are lower than -19 dB at 1550 nm for the slab width variations of ± 10 nm. The TM-to-TE conversion losses remain < 0.7 dB and the crosstalk values are < -16 dB for the nonlinearly-tapered waveguide width variations of ± 10 nm, as shown in Fig. 5(b). These results verify that the demonstrated PSR has a large fabrication tolerance to the waveguide width variations.

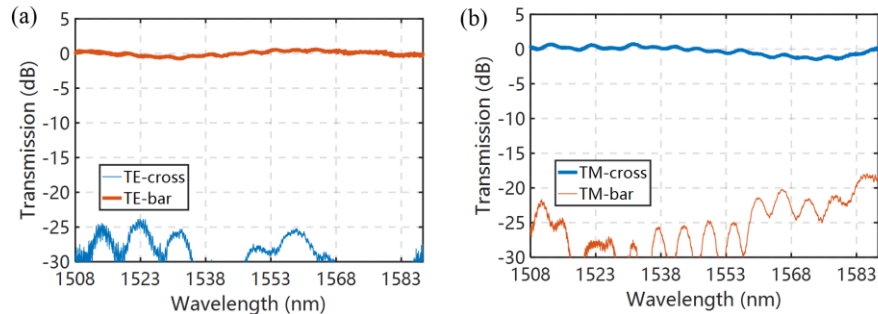


Fig. 4 Measured transmission responses of fabricated PSRs for (a) TE-polarization and (b) TM-polarization light inputs, respectively.

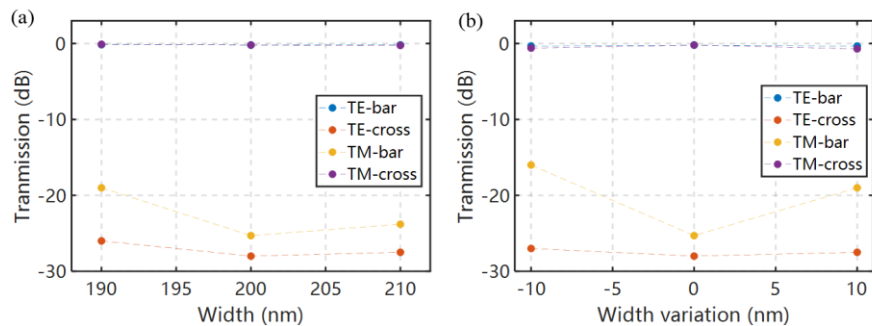


Fig. 5 Measured transmission of fabricated PSRs as a function of (a) slab width; (b) nonlinearly-tapered waveguide width variation.

4. Conclusions

We have experimentally demonstrated a silicon polarization splitter and rotator. Attributed to the nonlinearly-tapered coupler, adiabatic polarization splitting and rotating are achieved over a relatively short length of 129 μm . The insertion losses are < 1.4 dB and the crosstalk values are < -18 dB for both polarizations in the wavelength range of 80 nm. We also verify that the demonstrated PSR exhibits tolerance to waveguide width variations.

References

1. C. R. Doerr, L. Chen, D. Vermeulen, T. Nielsen, S. Azemati, S. Stulz, G. McBrien, X.-M. Xu, B. Mikkelsen, M. Givchchi, C. Rasmussen, and S. Y. Park, "Single-Chip Silicon Photonics 100-Gb/s Coherent Transceiver," Proc. OFC Th5C.1 (2014).
2. L. Liu, Y. Ding, K. Yvind, and J. M. Hvam, "Silicon-on-insulator polarization splitting and rotating device for polarization diversity circuits," Opt. Express **19**, 12646-12651 (2011).
3. Y. Ding, H. Ou, and C. Peucheret, "Wideband polarization splitter and rotator with large fabrication tolerance and simple fabrication process," Opt. Lett. **38**, 1227-1229 (2013).
4. D. Chen, X. Xiao, L. Wang, W. Liu, Q. Yang, and S. Yu, "Highly efficient silicon optical polarization rotators based on mode order conversions," Opt. Lett. **41**, 1070-1073 (2016).
5. D. Dai, and H. Wu, "Realization of a compact polarization splitter-rotator on silicon," Opt. Lett. **41**, 2346-2349 (2016).
6. Y. Ding, L. Liu, C. Peucheret, and H. Ou, "Fabrication tolerant polarization splitter and rotator based on a tapered directional coupler," Opt. Express **20**, 20021-20027 (2012).
7. Y. Zhang, Y. He, X. Jiang, B. Liu, C. Qiu, Y. Su, and R. A. Soref, "Ultra-compact and highly efficient silicon polarization splitter and rotator," APL Photon. **1**, 091304 (2016).
8. H. Guan, A. Novack, M. Streshinsky, R. Shi, Q. Fang, A. E.-J. Lim, G.-Q. Lo, T. Baehr-Jones, and M. Hochberg, "CMOS-compatible highly efficient polarization splitter and rotator based on a double-etched directional coupler," Opt. Express **22**, 2489-2496 (2014).
9. K. Tan, Y. Huang, G.-Q. Lo, C. Yu, and C. Lee, "Ultra-broadband fabrication-tolerant polarization splitter and rotator," Proc. Th1G.7 (2017).
10. C.-P. Ho, and S.-Y. Tseng, "Optimization of adiabaticity in coupled-waveguide devices using shortcuts to adiabaticity," Opt. Lett. **40**, 4831-4834 (2015).